

See discussions, stats, and author profiles for this publication at: <https://www.researchgate.net/publication/259200133>

# CdS Quantum Dots Doped Tuning of Deswelling Kinetics of Thermoresponsive Hydrogels Based on Poly(2-(2-methoxyethoxy)ethyl methacrylate)

ARTICLE *in* THE JOURNAL OF PHYSICAL CHEMISTRY B · DECEMBER 2013

Impact Factor: 3.3 · DOI: 10.1021/jp408164y · Source: PubMed

---

CITATIONS

7

READS

98

## 4 AUTHORS, INCLUDING:



Nagaraj Patil

University of Liège

3 PUBLICATIONS 22 CITATIONS

[SEE PROFILE](#)



Saswati Ghosh Roy

Indian Institute of Science Education and Re...

19 PUBLICATIONS 214 CITATIONS

[SEE PROFILE](#)

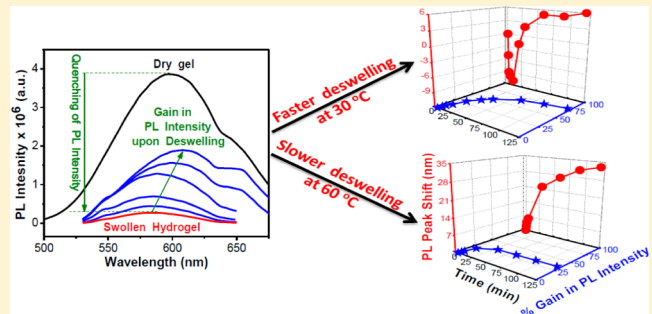
# CdS Quantum Dots Doped Tuning of Deswelling Kinetics of Thermoresponsive Hydrogels Based on Poly(2-(2-methoxyethoxy)ethyl methacrylate)

Nagaraj Patil, Saswati Ghosh Roy, Ujjal Haldar, and Priyadarsi De\*

Polymer Research Centre, Department of Chemical Sciences, Indian Institute of Science Education and Research, Kolkata, PO: BCKV Campus Main Office, Mohanpur 741252, Nadia, West Bengal, India

## S Supporting Information

**ABSTRACT:** Thermoresponsive poly(2-(2-methoxyethoxy)ethyl methacrylate) (PMEO<sub>2</sub>MA) based hybrid nanocomposite hydrogels (NCH) were synthesized by dispersing preformed cadmium sulfide (CdS) quantum dots (QDs) in the reaction mixture followed by polymerization via reversible addition–fragmentation chain transfer (RAFT) technique. High doping capacity and negligible QDs leakage were observed for hydrophilic QDs doped hydrogels (hpl-NCH) due to H-bonding interactions between QDs and pendant groups of hydrogel network. The hpl-NCH networks showed improved structural/orientational order and swelling ratios with increasing doping concentration compared to the organic hydrogel (OH). Opposite trends were observed for bulk-CdS (NCH-bulk) and 1-dodecanethiol capped CdS (NCH-DDT) doped hydrogels. Swelling induced linear retardance and quenching of photoluminescence (PL) intensity for hydrogels were exploited to study the deswelling kinetics respectively by Mueller matrix polarimetry and solid state fluorimetry, which were further corroborated with gravimetric analysis. For all the NCH, deswelling process significantly decreased with increasing temperature, which followed the order: 30 > 45 > 60 °C. Slower deswelling was observed for NCH-bulk and hpl-NCH compared to the OH, and also with increase in doping concentration due to the formation of skin layer. However, NCH-DDT exhibited accelerated deswelling process and the order was reversed with respect to doping concentration due to DDT mediated enhanced hydrophobic aggregation and water leakage channels created by long hydrophobic free-mobile nature of QDs surface tethered DDT molecules. The presented methodology provides tunable deswelling of PMEO<sub>2</sub>MA based hydrogels by doping with hydrophilically/hydrophobically modified CdS QDs.



## INTRODUCTION

Stimuli-responsive hydrogels are three-dimensional, water-insoluble, water-swelling, high molecular weight networks that change their physical properties abruptly with respect to the applied external stimuli, such as temperature, light, pH, enzyme, etc.<sup>1,2</sup> These smart materials show numerous attractive properties like defined morphology, high porosity, adjustable dimensions and the ability of their network to imbibe large amount of water, that makes them promising candidates for potential bioapplications due to resemblance of their micro-environment with the soft tissues.<sup>3,4</sup> The properties of pristine hydrogels can be reinforced by conjugating with inorganic nanobuilding blocks to obtain hybrid materials with unique functions and synergistic effect. These nanocomposite hydrogels (NCH) find various applications in biosensors, bioimaging, tissue engineering, drug delivery devices, etc.<sup>5–8</sup> Among them, the NCH containing quantum dots (QDs) have attracted tremendous interest in fundamental research and technical development because of photoluminescence behavior involving high quantum yield, large absorptivity, broad absorption spectrum, size and concentration dependent emission.<sup>9,10</sup>

Moreover, the integration of QDs into three-dimensional hydrogel matrix will not only offer protection to QDs against different harsh chemical environments but also provide unique photoelectronic properties to the resultant NCH, which could be useful for optoelectronics, catalysis and high-throughput assays for clinical applications as well as life science experiments.<sup>11–13</sup>

Recently, thermoresponsive hydrogels with short oligo(ethylene oxide) moiety were proposed as a promising alternative to poly(*N*-isopropylacrylamide) (PNIPAM) which is the most studied and applied in this research area.<sup>14–17</sup> Lutz et al. demonstrated and highlighted recent advances in the synthesis and application of thermoresponsive polymers and hydrogels based on oligo(ethylene glycol) (meth)acrylate monomers.<sup>18–24</sup> Numerous materials based on oligo(ethylene oxide) side chains are promising candidates for biomedical applications due to their water solubility, biocompatibility and

Received: August 15, 2013

Revised: November 27, 2013

nontoxicity. However, poly(2-(2-methoxyethoxy)ethyl methacrylate) (PMEO<sub>2</sub>MA) based hydrogels synthesized by controlled radical polymerization (CRP) techniques are prone to form skin layer at elevated temperatures,<sup>25–28</sup> above their volume phase transition temperature (VPT). This surface dense skin layer is impermeable to water molecules, thereby, retarding deswelling process, which might limit their applications. Several strategies have been adopted to improve the response rate of hydrogels, such as introducing dangling comb-chains,<sup>29</sup> forming porous/superporous structures,<sup>30,31</sup> adding polymer particles in the gel network,<sup>32</sup> cold-treating or freeze-drying the swollen hydrogel.<sup>33</sup> Also, it has been shown that NCH containing inorganic clay, either as cross-linker or filler, exhibits accelerated deswelling kinetics compared to pristine hydrogels.<sup>34,35</sup>

In the present work, we have synthesized NCH by dispersing preformed cadmium sulfide (CdS) QDs stabilized with or without small organic molecules in monomer solution, then polymerizing by reversible addition–fragmentation chain transfer (RAFT) polymerization of 2-(2-methoxyethoxy)ethyl methacrylate (MEO<sub>2</sub>MA). The quantity and nature of doped QDs is expected to alter the swelling ratios and deswelling kinetics, due their functional interaction with the pendent groups of hydrogel network. Synthesis of QDs, QDs doped hydrogels and their photophysical properties are extensively considered elsewhere.<sup>11,12,36</sup> However, the systematic comparison of effect of added QDs content and nature, on skin layer formation and hence the deswelling kinetics is scarce, which has become main focus of the present work. The macroscopic deswelling was studied by conventional gravimetric analysis, fluorimetry and further corroborating with Mueller matrix polarimetry (MMP) method.<sup>37–40</sup>

## ■ EXPERIMENTAL SECTION

**Materials.** CdCl<sub>2</sub>·2.5H<sub>2</sub>O (98%), Na<sub>2</sub>S·9H<sub>2</sub>O (98%), 2-mercaptopropanoic acid (3MPA, 99%), 1-dodecanethiol (DDT, 98%), sodium diethyl sulfosuccinate (AOT, 98%), anhydrous *N,N*-dimethylformamide (DMF, 99.9%), and anhydrous toluene (99.8%) were purchased from Sigma-Aldrich and used as received. The MEO<sub>2</sub>MA (Aldrich, 95%), di(ethylene glycol)dimethacrylate (DEGDMA, Aldrich, 95%) were purified prior to polymerization by passing through a column of basic alumina. The 2,2'-azobis(isobutyronitrile) (AIBN, Aldrich, 98%) was recrystallized twice from methanol. The chain transfer agent (CTA), 4-cyano-4-(dodecylsulfanylthiocarbonyl)sulfanylpentanoic acid (CDP), was synthesized as reported elsewhere.<sup>28</sup> The solvents such as diethyl ether and ethanol were purified by standard procedures. HPLC grade water was used for final dialysis. Synthesis of QDs<sup>41,42</sup> and QDs doped hydrogels are provided in the Supporting Information.

**Characterization Methods.** UV-visible studies were made using the Perkin-Elmer Lambda 35 UV/vis Spectrometer with a scan rate of 500 nm/min. Perkin-Elmer Spectrum 100 FT-IR spectrometer was used to record IR spectra. The thermogravimetric analysis (TGA) was performed on a Mettler Toledo TGA/SDTA 851e instrument at a heating rate of 10 °C min<sup>-1</sup> with a sample weight of ~10 mg in N<sub>2</sub> atmosphere. Photoluminescence spectra were recorded on a Horiba Jobin Yvon FluoroMax-4 spectrofluorometer with a right-angle geometry, using 1 cm quartz cuvettes for solution samples, and J1933 solid-sample holder at a 45° angle for gels. Macroscopic deswelling kinetics was studied by conventional gravimetry, fluorimetry and MMP. More details about the use

of MMP to study deswelling kinetics can be found in our previous publication.<sup>28</sup> Field emission scanning electron microscopy (FE-SEM) study was performed on a Carl Zeiss-Sigma instrument. Small pieces of dried hydrogel samples were immersed in DI-water for 2 days at 5–8 °C to reach its maximum swollen state. Then, the swollen hydrogels were frozen in liquid N<sub>2</sub> and quickly freeze-dried in lyophilizer (Orleon instrument) under high vacuum at -50 °C for 32 h. The freeze-dried hydrogels were coated on very thin layer of gold for 1 min under high vacuum and examined by FE-SEM.

**Kinetic Studies upon Deswelling.** Deswelling kinetics can be defined as temporal change in water content of gels, which can be expressed in terms of swelling ratio (eq 1) and water retention (eq 2). Swelling ratio is defined as weight of water contained within swollen hydrogel with respect to its dry weight ( $W_d$ ). Water retention is the ability of hydrogel to retain certain amount of water with respect to its initial amount of water absorbed. Similarly, % quenching/gain in PL intensity and % retention in linear retardance are defined according to the eqs 3, 4, and 5, respectively.

$$\text{swelling ratio} = \frac{(W_t - W_d)}{W_d} \quad (1)$$

$$\text{water retention} = \frac{(W_t - W_d)}{(W_0 - W_d)} \quad (2)$$

$$\% \text{quenching of PL intensity} = \frac{(I_d - I_0)}{I_d} \times 100 \quad (3)$$

$$\% \text{gain in PL intensity} = \frac{(I_t - I_0)}{(I_d - I_0)} \times 100 \quad (4)$$

$$\% \text{retention in linear retardance} = \frac{(\delta_t - \delta_d)}{(\delta_0 - \delta_d)} \times 100 \quad (5)$$

where  $W_t$ ,  $I_t$ , and  $\delta_t$  are respectively weight, PL intensity, and linear retardance of hydrogel at time  $t$ , and  $W_0$ ,  $I_0$  and  $\delta_0$  are respectively weight, PL intensity and linear retardance of equilibrium swollen hydrogel below the VPT and the VPT of PMEO<sub>2</sub>MA network in water was reported to be 26 °C.<sup>26</sup> A rectangular piece of hydrogel was immersed in DI-water maintained at 6 °C and left to swell. After ensuring no weight change with respect to time, the hydrogel was transferred to a preheated water bath either at 30, 45, or 60 °C. At regular time intervals the gel was taken out, wiped out with blotting paper, weighed and placed again in the same bath.

## ■ RESULTS AND DISCUSSION

**Synthesis.** CdS QDs without the capping agent and capped with 2ME, 3MPA, and DDT were investigated by FT-IR studies (Figure 1). In CdS-2ME, CdS-3MPA, and CdS-DDT, the absorption peaks at 2922, 2851 cm<sup>-1</sup> ( $\nu_{\text{C}-\text{H}}$ ) and 1462 cm<sup>-1</sup> ( $\nu_{\text{CH}_2}$ ) can be assigned to the methyl and methylene asymmetric stretching modes from the capping agents, respectively. For CdS-2ME (Figure 1B), the absorption peaks at 1418, 1063, and 1118 cm<sup>-1</sup> can be attributed to the O–H deformation, alcohol CH<sub>2</sub>–OH and C–O primary stretching, respectively. The signals for CdS-3MPA (Figure 1C) at 1712 and 1546 cm<sup>-1</sup> are due to the protonated C=O and deprotonated antisymmetric carboxylate stretches, respectively. In addition, absence of S–H absorption at ~2572 cm<sup>-1</sup> and

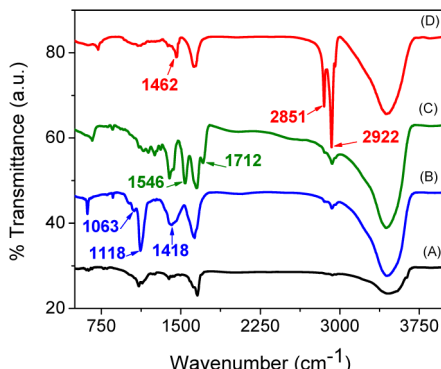


**Figure 1.** FT-IR spectra of (A) CdS-bulk, (B) CdS-2ME, (C) CdS-3MPA, and (D) CdS-DDT.

presence of CdS-bulk peaks in all cases successfully proves the capping of ligands to CdS QDs.<sup>43–45</sup>

The UV-vis absorption spectra of capped QDs in solution (Figure 2A) exhibits absorption edge, that is blue-shifted with respect to the bulk CdS (~508 nm), arising from quantum confinement effect in the nanoparticles.<sup>46</sup> The size of particles, calculated using Henglein's empirical curve,<sup>47,48</sup> are tabulated in Table S1 (in the Supporting Information), indicating 3MPA better stabilizing agent compared to 2ME and DDT. Also, the peak position of emission maxima of capped QDs blue-shifted compared to CdS-bulk (Figure 2B), according to the size of QDs. Thermal properties of all the samples were investigated by TGA under nitrogen (Figure 3). CdS-bulk exhibited good thermal stability with insignificant weight-loss (less than 4.5%) up to 500 °C, whereas 17.4, 18.2, and 21.1% weight loss have been observed respectively for CdS-2ME, CdS-3MPA, and CdS-DDT, which correspond to the capping agents. Therefore, the combined results of FT-IR, TGA, UV-vis, and fluorescence studies reveal the success of small organic molecules to cap CdS QDs.

On the basis of the previous research,<sup>28</sup> we have used CDP as RAFT agent to synthesize NCH with well-defined hydrogel networks. Successful encapsulation of QDs in the hydrogel matrix was confirmed by TGA, FE-SEM and photoluminescence (will be discussed in subsequent paragraphs) studies. From TGA, 1.6, 1.9, 2.0, and 2.2 wt % residual weights were observed above 450 °C, respectively, for NCH-bulk-2.0, NCH-DDT-2.0, NCH-2ME-2.0, and NCH-3MPA-2.0, which corresponds to the immobilized CdS core in the hydrogel matrix (Figure 3). Above 450 °C, we observed residual weight of ~1%

in the case of OH, which may correspond to the organic carbon residues trapped in the TGA pan. Hydrogels doped with CdS-2ME and CdS-3MPA exhibited high doping capacity and negligible QDs leakage, which can be attributed to the H-bonding interactions<sup>48,50</sup> between QDs surface tethered 2ME (–OH) and 3MPA (–COOH) ligands with ethereal oxygen atoms of pendant oligo(ethylene oxide) chains. In contrast, a relatively weak hydrophobic interactions between DDT of CdS and apolar hydrogel backbone, resulted in a small amount of QDs leakage (5%) in the case of NCH-DDT-2.0.<sup>51</sup> However, absence of secondary interactions between CdS-bulk and hydrogel matrix (physical entrapment of QDs in cross-linked hydrogel matrix), caused 20% QDs leakage in the case of NCH-bulk-2.0.

**Hydrogel Structure and Swelling Ratio.** Gravimetrically measured equilibrium swelling ratios of hydrogels measured at 10 °C (below VPT) are summarized in Table 1. Among NCH with same feed ratio, hpl-NCH (NCH-3MPA > NCH-2ME) showed higher swelling ratio compared to OH, and swelling ratio increased with the doping concentration from 0.5 to 2.0 wt %. Whereas, hpb-NCH had lower swelling ratio than OH, and swelling ratio decreased with increasing doping concentration. This opposite trend might suggest that overall hydrophilicity and the inherent/induced network structure decides water absorbing capacity of hydrogels. Mueller matrix polarimetry has proven to be a valuable technique to understand the orientation and structure of hydrogel networks.<sup>28</sup> The Mueller matrices recorded from the hydrogel matrices (wavelength range 525–725 nm) were subjected to Mueller matrix decomposition analysis to yield quantitative individual polarimetry parameters, namely, linear retardance ( $\delta$ ) and diattenuation ( $d$ ). In our previous paper<sup>28</sup> we described in detail the qualitative meaning and origin of  $\delta$  and  $d$ -parameters in hydrogels. Briefly, at macroscopic level  $\delta$  and  $d$  arise from differences in refractive indices for different polarization states due to organization of individual anisotropic domains. Additionally, scattering, reflection/transmission of light through layered structures may also contribute to diattenuation effects. The organization of pore structures<sup>52</sup> and suppression of segmental mobilities of polymer chains because of significant spatial restrictions (cross-linking reactions) minimizes polymer chain randomization, which may lead to appreciable retardance and diattenuation effects in the dry gel (Table 1 and Figures S1–S10 Supporting Information).

The magnitudes of  $\delta$  and  $d$ -parameters were observed to be higher for the hpl-NCH (NCH-3MPA > NCH-2ME)

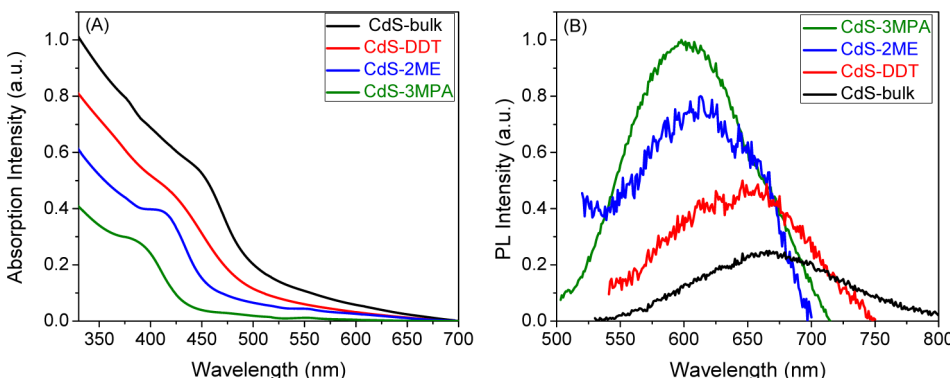


**Figure 2.** UV-vis absorption (A) and photoluminescence (B) spectra of QDs in solution.

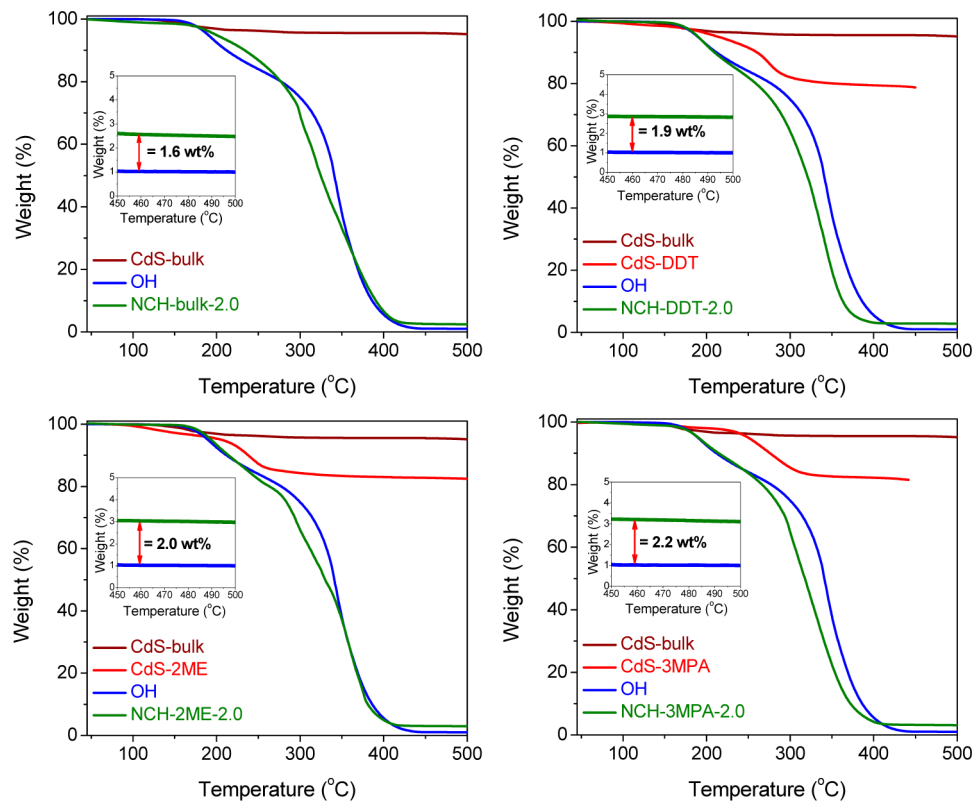


**Figure 3.** TGA curves of samples at a heating rate of 10 °C/min under N<sub>2</sub> atmosphere. Inset: residual weight of QDs core in NCH above 450 °C.

**Table 1. Swelling, Optical and Photo-Physical Properties of Hydrogels**

run	dry gels			swollen hydrogels			swelling ratio <sup>b</sup>	% quenching of PL intensity <sup>c</sup>
	( $\delta$ ) <sup>a</sup> (rad)	( $d$ ) <sup>a</sup>	$\lambda_{\text{emission}}$ (nm)	( $\delta$ ) <sup>a</sup> (rad)	( $d$ ) <sup>a</sup>	$\lambda_{\text{emission}}$ (nm)		
OH	0.08	0.08	—	1.54	0.39	—	6.1	—
NCH-3MPA-0.5	0.10	0.09	595	1.77	0.42	583	7.1	93.1
NCH-3MPA-1.0	0.13	0.10	595	2.0	0.48	577	8.2	96.9
NCH-3MPA-2.0	0.15	0.13	596	2.31	0.62	578	9.4	98.7
NCH-2ME-0.5	0.08	0.08	605	1.70	0.40	599	6.7	86.7
NCH-2ME-1.0	0.10	0.09	606	1.85	0.42	~598	7.4	93.5
NCH-2ME-2.0	0.13	0.11	607	2.16	0.47	~596	8.5	96.5
NCH-DDT-0.5	0.05	0.05	622	1.36	0.31	—	5.8	—
NCH-DDT-1.0	0.04	0.03	623	1.13	0.21	—	5.3	—
NCH-DDT-2.0	0.03	0.02	624	1.00	0.10	—	4.5	—
NCH-bulk-0.5	0.06	0.06	672	1.41	0.33	658	6.1	78.8
NCH-bulk-1.0	0.05	0.04	675	1.21	0.30	~660	5.8	75.6
NCH-bulk-2.0	0.04	0.03	683	0.95	0.23	~662	5.4	65.7

<sup>a</sup>Mueller matrix-derived  $\delta$  and  $d$ -parameters at  $\lambda = 633$  nm. <sup>b</sup>Calculated according to eq 1. <sup>c</sup>Calculated according to eq 3 for swollen NCH in comparison with dry gels.

compared to OH. The easiness of lining of pendant monomer groups would be another important parameter, which decides their orientation, and hence the structural order of hydrogel networks. The nonlinearity of oligo(ethylene oxide) units in MEO<sub>2</sub>MA and large internal degree of freedom due to free-rotating bonds in the pendant groups makes them to orient randomly, thereby reducing the structural order in the case of OH. The bridging of QDs in between monomers and random networks, due to H-bonding interactions between QDs surface tethered  $-\text{OH}/-\text{COOH}$  and ethereal oxygen atoms of pendant oligo(ethylene oxide), might minimize the randomization of pendant groups and random networks, leading to enhancement in  $\delta$  and  $d$ -parameters. With increase in doping

concentration, both  $\delta$  and  $d$ -parameters increased ( $2.0 > 1.0 > 0.5$ ), suggesting H-bonding was predominantly intermolecular between QDs and hydrogel networks. The decrease in the values of  $\delta$  and  $d$ -parameters with the concentration, in case of NCH-bulk and NCH-DDT suggests their presence in the gel matrices as added structural heterogeneity, due to lack of functional interactions. This phenomenon is schematically represented in Scheme 1 for NCH and corresponding representation for OH is given in Scheme S1.

Figure 4 shows the morphology of NCH and OH by FE-SEM imaging technique in cross-section mode. The consequence of QDs doping into hydrogel matrix, can also be seen from these images, scrutinising distribution of pores. A uniform

**Scheme 1.** Cartoon Representation of NCH Structures in Dry, Swollen, and Deswollen States

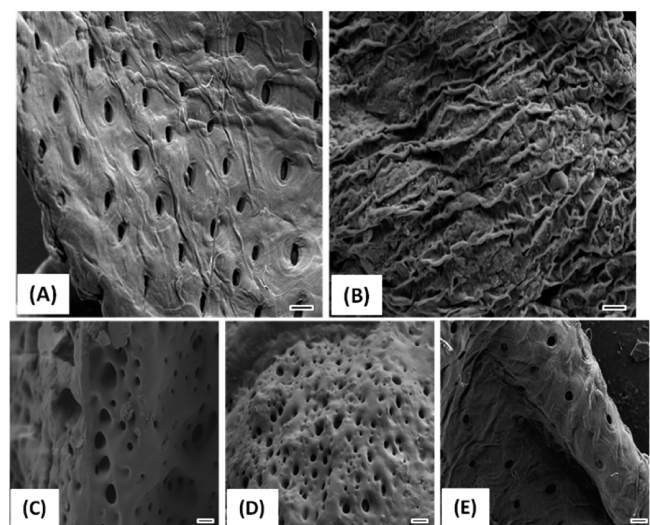
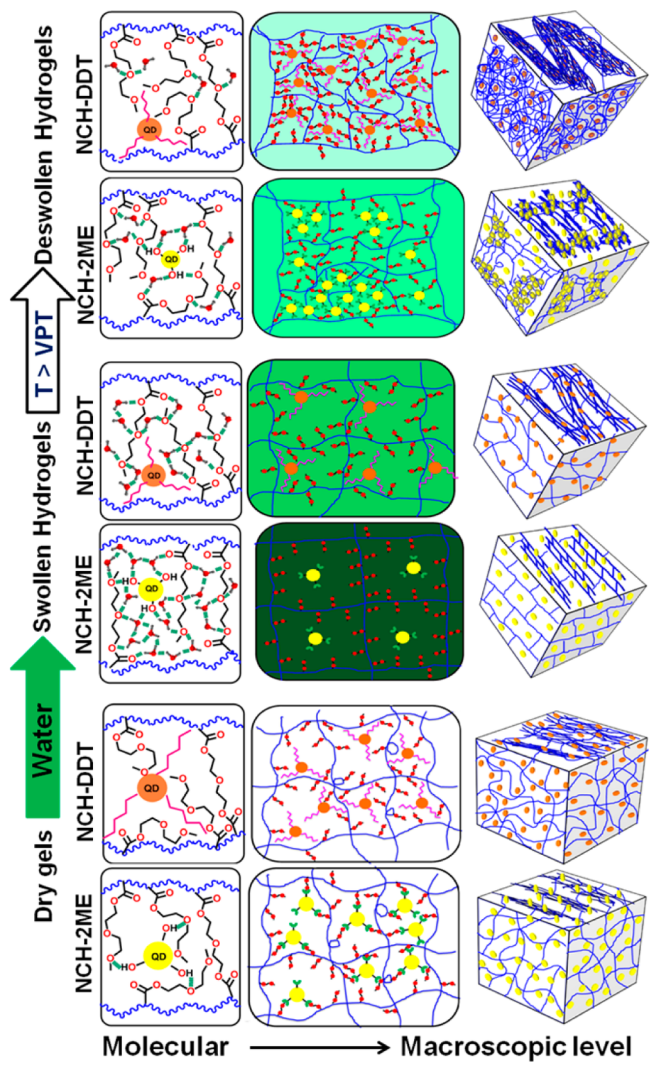


**Figure 4.** FE-SEM images of (A) NCH-3MPA-1.0, (B) NCH-DDT-1.0, (C) NCH-2ME-1.0, (D) NCH-bulk-1.0, and (E) OH. In all the cases, scale bars represent 2  $\mu$ m.

distribution of pores observed for OH, NCH-3MPA-1.0, and NCH-2ME-1.0. Whereas, NCH-bulk-1.0 was characterized by random pores distribution. Interestingly, we noticed wrinkle-shaped, long-ridges with random distribution of pores in NCH-DDT-1.0 (Figure 4B). Therefore, the doping of verities of QDs into hydrogel matrix, and hence their ability to induce different NCH structures, decides swelling ratio (Table 1) and deswelling fate (described in subsequent paragraphs) of these smart materials.

All the hydrogels below VPT exhibited swelling induced linear retardance and diattenuation effects (Table 1, Figures S1–S10). Significantly higher magnitudes of  $\delta$  and  $d$  in the swollen hydrogels can be attributed to the fact that hydration causes alignment of nonlinear oligo(ethylene oxide) analogues in the pendant groups of  $\text{MEO}_2\text{MA}$  due to bridging of water molecules between neighboring pendant groups, and also between the random networks and hence throughout the gel. The overall increase in hydrophilicity and structural order of hpl-NCH ( $\text{NCH-3MPA} > \text{NCH-2ME}$ , and also with concentration ( $2.0 > 1.0 > 0.5$ )), resulted in increased water uptake and enhanced bridging of water molecules to yield a hydrogel with improved structural order compared to OH (Table 1). Interestingly, the magnitudes of  $\delta$  and  $d$ -parameters were low for NCH-DDT ( $0.5 > 1.0 > 2.0$ ) compared to OH. Lower swelling ratio and reduced formation of layered arrangement (lower values of  $d$  both in the dry and swollen state) could be ascribed to the superhydrophobic nature (low surface free energy) of long-chain alkyl groups of DDT molecules on CdS surface.<sup>53,54</sup>

The PL spectra of dry and swollen NCH are shown in Figures 5 and 6 and also in Figures S11–S12 in the Supporting Information. The peak positions of PL were blue-shifted for all doping concentrations in case of NCH-DDT, NCH-2ME, and NCH-3MPA compared to colloidal QDs solutions (Table S1). At different doping concentrations, we did not observe noticeable change in the peak position of PL (within the experimental error, Table 1). Furthermore, the enhancement in PL intensity with the doping concentration (Figures 5A and S11A and S12A) implies that the secondary interactions (H-bonding/hydrophobic) between QDs and hydrogel matrices could further passivate the surface of the QDs (physical immobilization of QDs in topologically constrained cross-linked gel matrix) and effectively diminish the contribution of nonradiative channels for electron–hole recombination. The decrease in PL intensity with apparent red-shift in peak position of PL with the doping concentration (Figure 6A), in case of NCH-bulk compared to CdS-bulk, clearly suggests concentration quenching effects, due to energy transfer between different sized particles in close-packed crystals (physical contact between QDs).<sup>55–57</sup> The presence of shoulder at higher wavelength in NCH (~650 nm) might be due to the aggregation of QDs during synthesis and/or purification process. Swollen NCH exhibited further blue-shift in PL peak position compared to dry gels, because of uniform QDs distributions in more homogeneous swollen hydrogel network (Scheme 1 and Table 1, higher magnitude of  $\delta$  and  $d$ -parameters compared to dry gels). A large quenching of PL intensity was observed for swollen hydrogels, which was proportional to their swelling ratios (Table 1). Weakening of the topological constraints on immobilized QDs and their migration into the absorbed water resulted in excited state energy transfer to high dielectric constant water molecules, causing quenching of PL intensity. However, no trap-state PL

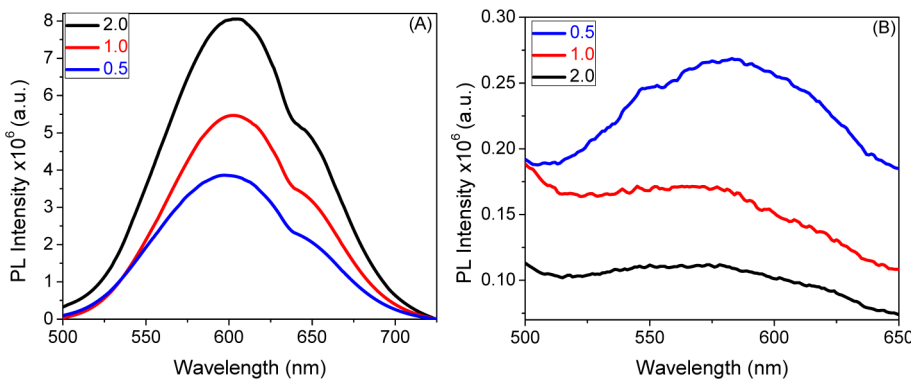


**Figure 5.** PL spectra of NCH-3MPA for (A) dry gels and (B) swollen hydrogels with different wt % of QDs.

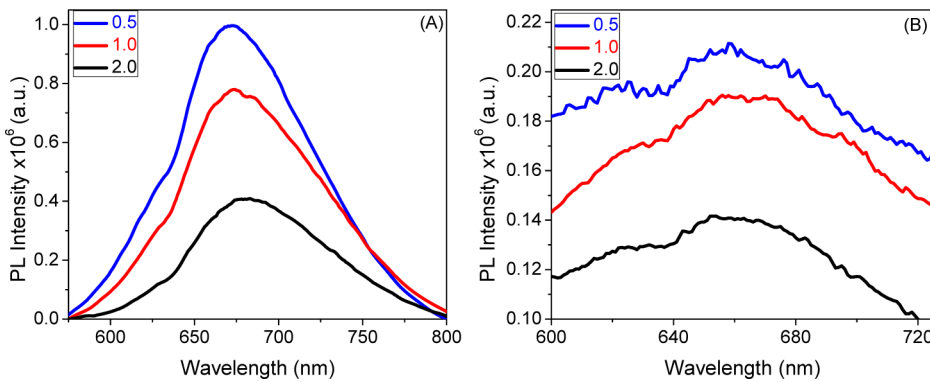


**Figure 6.** PL spectra of NCH-bulk for (A) dry gels and (B) swollen hydrogels with different wt % of QDs.

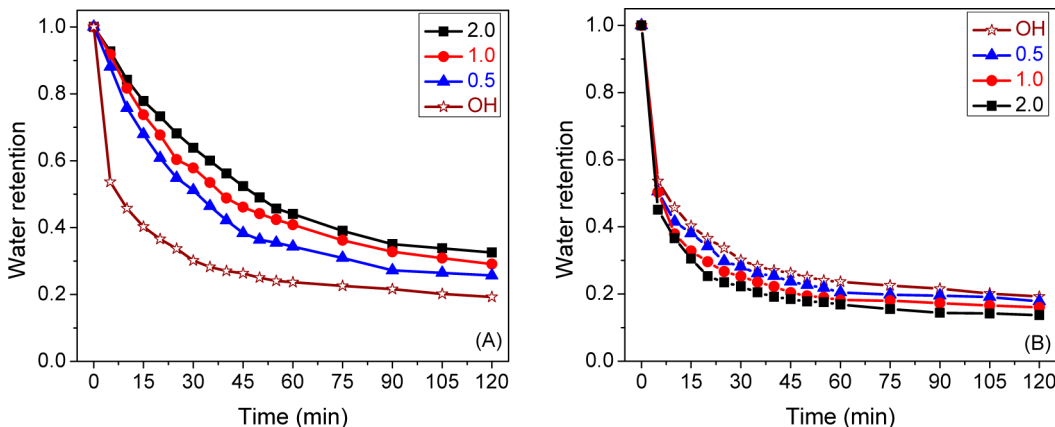


**Figure 7.** Comparison of water retention upon deswelling at 30 °C for (A) NCH-3MPA and (B) NCH-DDT with different wt % of QDs.

emission was observed for swollen NCH-DDT, may be due to incompatibility between hydrophobic QDs and hydrophilic hydrogel matrix below VPT.

**Deswelling Kinetic Studies.** Deswelling kinetics of hydrogels above VPT was studied at 30, 45, and 60 °C by recording the decrease of weight as a function of time (conventional gravimetry), which was converted to the decrease of water retention using eq 2. The decrease of water retention against time for OH at different temperatures is shown in Figure S13. The OH exhibited accelerated deswelling at 30 °C (close to VPT), whereas deswelling was significantly retarded at higher temperatures (45 and 60 °C). The detailed comparative mechanistic insights into the deswelling process are discussed elsewhere.<sup>26,28</sup> Relatively fast volume phase transitions at higher temperatures leads to the formation of

surface dense skin layer at gel-water interface, which is impermeable to water molecules. Hence, hydrogels synthesized by CRP are characterized by large water retention values, which could hamper their application at higher temperatures. Therefore, the main focus of the present work is to understand and tune the deswelling process of hydrogels by doping with QDs.

Variation of water retention with time at 30 °C for NCH-3MPA and NCH-DDT are shown respectively in parts A and B of Figure 7, which show that NCH-DDT attained stable water retention value faster with increased amount of water loss ( $2.0 > 1.0 > 0.5$ ) compared to OH. Whereas, deswelling of NCH-3MPA was slower and the order was reversed. From the deswelling mechanistic point of view, the volume phase transition properties of hydrogel at temperatures above VPT

largely depend on the extent of polymer–polymer interactions, decided by their hydrophobic aggregations during dehydration. The effect of polymer chain mobilities on dehydration process can be visualized by H-bonded structure in hpl-QDs doped hydrogels. The steric hindrance due to QDs mediated, rigid extended H-bonded network, could retard the dehydration and subsequent hydrophobic aggregation of polymer chains, thereby, retaining water molecules for a longer time. Whereas in the case of NCH-DDT, overall increase in hydrophobic surface area<sup>58</sup> ( $2.0 > 1.0 > 0.5$ ) resulted in a faster deswelling process due to the long-hydrophobic DDT on CdS surface, which might accelerate the hydrophobic aggregation of dehydrated polymer chains, because of free-mobile nature of alkyl end. Also, it is known that long-dangling-graft chains create hydrophobic cores, which could provide water leakage channels for water molecules to diffuse out.<sup>59,60</sup> Hence, combined effect of enhanced hydrophobic contact area and water leakage channels might accelerate the deswelling process of NCH-DDT. To justify the proposed mechanism, we studied the deswelling of NCH-2ME at 30 °C (Figure S14A). Similar trend was observed with improved deswelling process compared to NCH-3MPA, due to better mobility of dehydrating chains, which is consistent with lower H-bonded network structure (lower  $\delta$  and  $d$ -parameters in dry and swollen state) compared to NCH-3MPA observed by Mueller matrix polarimetry and swelling ratio studies (Table 1). Interestingly, for NCH-3MPA and NCH-2ME-2.0, nearly a linear deswelling process was observed until they lost ~60% of water (which might coincide with controlled pseudo first order release profile, whereas OH and NCH-DDT were characterized by immediate release of water). The linear coefficient of slope seemed to decrease with increase in doping concentration, signifying release kinetics of loaded hydrophilic drugs in hydrogel matrix, can be tuned by varying H-bonding concentration. Hydrogels doped with CdS-bulk did not improve the deswelling process (Figure S14B) compared to OH, suggesting ligands present on the QDs surface play crucial role rather than CdS core. The CdS-bulk is expected to be accommodated in the hydrophilic domains of hydrogel, retaining water molecules for a longer time.<sup>36</sup>

During the deswelling process,  $\delta$  decreased with time, due to destructuring of induced H-bonded structure in the swollen hydrogel, which we have exploited to study deswelling kinetics quantitatively by Mueller matrix polarimetry,<sup>28</sup> and established a linear dependence of  $\delta$  with absolute amount of water loss. Therefore, gravimetric deswelling analysis can be further corroborated with % retention in linear retardance (%  $\delta_R$ ) values (eq 5) and has been summarized in Table 2 ( $\delta$  as a function of  $\lambda$  at deswelling time  $t = 120$  min, are shown in Figures S15–S19). It was observed that %  $\delta_R$  increased with doping concentration for hpl-NCH (3MPA > 2ME) at 30 °C compared to OH, which was in accordance with the water retention values. Higher the amount of water retention, lesser the loss of induced H-bonded structure, and slower the deswelling process. In contrast, %  $\delta_R$  decreased with doping concentration for NCH-DDT compared to OH and hpl-NCH, inferring accelerated deswelling process.

Gravimetric deswelling plots for NCH-3MPA and NCH-DDT at 45 and 60 °C are shown in Figures 8 and 9, respectively. In general, deswelling process was significantly retarded at 45 and 60 °C ( $60^\circ\text{C} > 45^\circ\text{C}$ ) for all NCH compared to deswelling at 30 °C. More retardation to the deswelling process was observed for hpl-NCH (NCH-3MPA >

**Table 2. Mueller Matrix-Derived  $\delta$ -Parameter for Deswollen hydrogels at Different Temperatures**

run	30 °C		45 °C		60 °C	
	$\delta$ (rad) <sup>a</sup>	$\delta_R$ <sup>b</sup> (%)	$\delta$ (rad) <sup>a</sup>	$\delta_R$ <sup>b</sup> (%)	$\delta$ (rad) <sup>a</sup>	$\delta_R$ <sup>b</sup> (%)
OH	0.34	17.8	0.77	47.2	0.88	54.8
NCH-3MPA-0.5	0.49	23.2	0.90	47.9	1.12	62.9
NCH-3MPA-1.0	0.63	26.7	1.36	65.8	1.50	73.3
NCH-3MPA-2.0	0.79	29.7	1.81	76.8	1.99	85.6
NCH-2ME-0.5	0.44	22.2	0.79	44.4	0.99	56.1
NCH-2ME-1.0	0.54	25.2	0.96	49.1	1.24	65.1
NCH-2ME-2.0	0.73	29.5	1.36	60.6	1.71	77.8
NCH-DDT-0.5	0.21	12.2	0.48	32.8	0.58	40.5
NCH-DDT-1.0	0.17	11.8	0.32	25.6	0.37	30.2
NCH-DDT-2.0	0.12	9.27	0.21	18.5	0.21	18.6
NCH-bulk-0.5	0.31	18.5	0.68	45.9	0.85	58.5
NCH-bulk-1.0	0.28	19.8	0.75	60.3	0.86	69.0
NCH-bulk-2.0	0.26	24.4	0.75	78.0	0.80	83.5

<sup>a</sup>Mueller matrix-derived linear retardance ( $\delta$ ) parameters at  $\lambda = 633$  nm during deswelling at time  $t = 120$  min. <sup>b</sup>Calculated according to eq 5.

NCH-2ME (Figures S20–S21A), and also with doping concentrations compared to OH, which can be explained by the formation of skin layer. The skin layer forming ability largely depends on temperature of deswelling and network structure. Volume phase transitions are relatively fast at elevated temperatures (45/60 °C), resulting in rapid dehydration of chains situated at the water-gel interface followed by faster hydrophobic aggregation to form a surface-dense thick skin layer, which is impermeable to water molecules, thereby, retarding the deswelling rate because the water molecules have to leak through generated cracks after rupturing of the skin layer. Since this phenomenon was enhanced more at 60 °C compared to 45 °C, slower deswelling was observed at 60 °C. As established in the earlier sections, the structure, homogeneity and also layered arrangement ( $\delta$  and  $d$ -parameters in Table 1 for dry and swollen hydrogels) of hpl-NCH (NCH-3MPA > NCH-2ME) is proportional to the QDs doping concentration, consequently, the order of vulnerability to form skin layer and hence, retarded deswelling is  $2.0 > 1.0 > 0.5$ . The NCH-bulk (Figures S20–S21B) also exhibited slower deswelling compared to OH. In contrast, improved deswelling was observed in the case of NCH-DDT (Figures 8B and 9B) and the order was reversed compared to hpl-NCH. DDT mediated hydrophobic aggregations of dehydrating polymer chains and the mobility of dangling-graft chains to create hydrophobic cores would be more pronounced at higher temperature ( $60^\circ\text{C} > 45^\circ\text{C}$ ) due to greater conformational degree of freedom at elevated temperature. Since the order of hydrophobicity and number of dangling chains in NCH-DDT was  $2.0 > 1.0 > 0.5$ , more number of water leakage channels were created in the same order, providing leakage channels through skin layer for water molecules to diffuse out. Note that skin layer forming ability was reduced to a large extent in the case of NCH-DDT ( $2.0 > 1.0 > 0.5$ ) due to long DDT molecules on CdS surface, as supported by lower value of  $d$  (Table 1), inferring feeble layered arrangement compared to OH. In general values of %  $\delta_R$  (Table 2) increased with increase in deswelling temperature ( $60 > 45 > 30$  °C) for all hydrogels, and also with the doping concentration for hpl-NCH (3MPA > 2ME). But this order with respect to doping concentration was

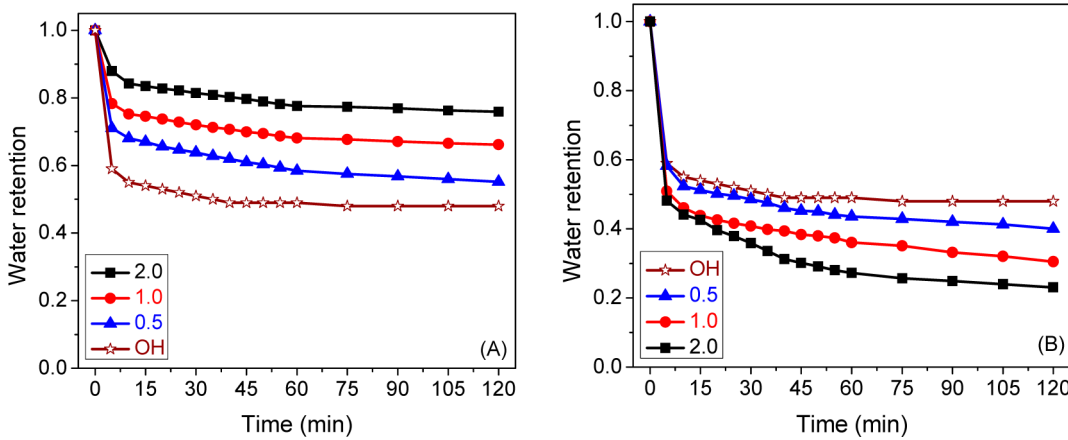


Figure 8. Comparison of water retention upon deswelling at 45 °C for (A) NCH-3MPA and (B) NCH-DDT gels with different wt % of QDs.

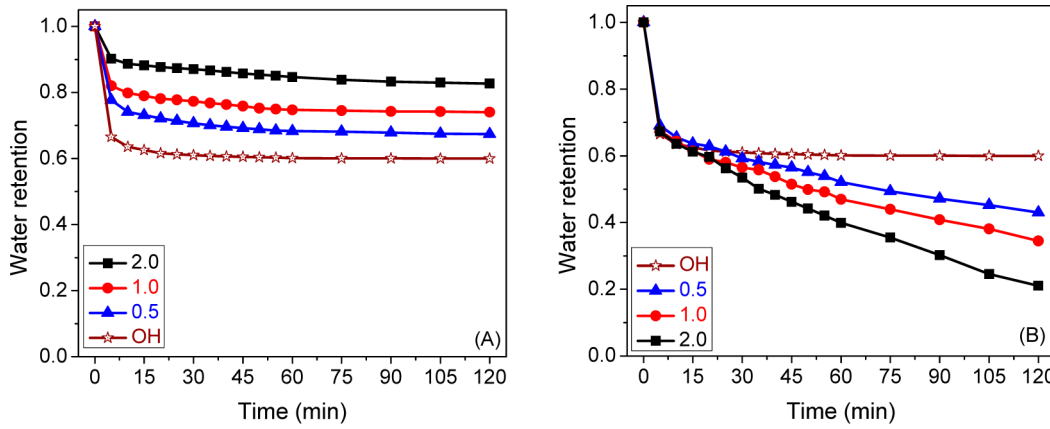


Figure 9. Comparison of water retention upon deswelling at 60 °C for (A) NCH-3MPA and (B) NCH-DDT with different wt % of QDs.

reversed for NCH-DDT, supporting gravimetric deswelling analysis results. Significant penetration of water molecules into the interior of the collapsed gel, due to the formation of skin layer, facilitated to retain the swelling induced linear retardance at higher temperatures, which was in accordance with water retention values.<sup>28</sup>

The spectral properties of QDs depend to some extent upon their surrounding local environment. Embedding QDs in thermoresponsive hydrogel might result in change of their PL intensity and/or position of peak emission, with change in temperature, deswelling time, doping concentration, etc. Thus, embedding QDs in smart hydrogel matrices may be an efficient way of enhancing their functionality and can also be exploited to probe changes in the local embedding environment. The % gain in PL intensity (eq 4) was plotted as a function of time upon deswelling for NCH-3MPA-0.5 (Figure 10), and the corresponding PL plots are shown in Figure S22. The enhancement in PL intensity was observed upon deswelling and the curves were qualitatively similar to gravimetric deswelling plots, inferring slower deswelling in case of NCH-3MPA-0.5 compared to NCH-2ME-0.5 and also with an increase in temperature (Figure S23A; corresponding PL plots in Figure S24). NCH-bulk-0.5 also demonstrated a similar trend (Figure S23B; corresponding PL plots in Figure S25). This PL enhancement is presumably due to change in configuration of the hydrogel that restricts the migration of QDs, due to fixation of molecular motions of QDs upon deswelling, which minimizes the nonradiative energy loss paths.

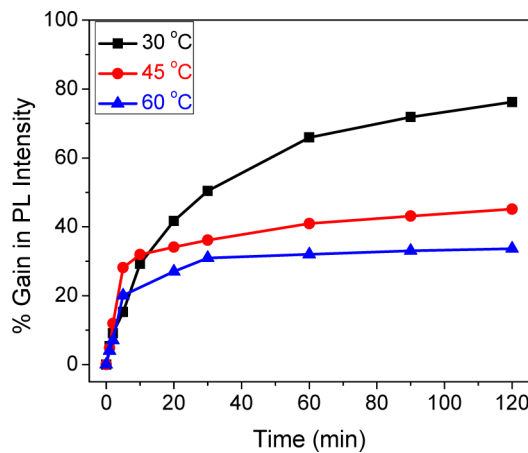


Figure 10. Percent gain in fluorescence intensity, upon deswelling, for NCH-3MPA-0.5 at different temperatures.

Therefore, the maximum % gain in PL intensity at 30 °C suggests significant increase in fixation of QDs in the matrix and less nonradiative energy transfer from the excited state QDs to water molecules (low water retention value at deswelling time  $t = 120$  min), compared to 45 and 60 °C. However, substantial expansion of hydrophobic domains at the cost of hydrophilic domains, upon deswelling created hydrophobic pockets where hydrophobic QDs can reside, which resulted in apparent gradual increase in PL intensity for NCH-

DDT-0.5 (Figure S26). Since swollen NCH-DDT did not exhibit pronounced PL emission, we did not study systematic deswelling kinetics by fluorimetry. Nevertheless, a gradual increase in PL intensity upon deswelling at all temperatures and comparable PL intensity at deswelling time  $t = 120$  min to that of dry gel (ca.  $\sim 1.65 \times 10^6$  a.u.), indicated accelerated deswelling process compared with hpl-NCH. Note that enhancement in PL intensity upon deswelling was observed, despite the increase in scattering from the hydrogel matrix above VPT, where the gel becomes turbid and acts as a strong scattering center.

On the other hand, a more interesting phenomenon of the PL peak position shift was observed with the temperature. It is well-known that PL peaks of QDs shift to longer wavelength with larger particle size.<sup>61</sup> The possibility of growth of QDs during gel synthesis was excluded according to Li et al.<sup>62</sup> There could be two possible reasons for the shift in PL peak position. Thermoresponsive volume phase transitions above VPT, results in change in the microenvironment, especially the dielectric constant ( $\epsilon$ ) of the QDs embedded in the PMEO<sub>2</sub>MA matrices. Second, homogeneous to heterogeneous transformation of hydrogel network takes place upon shrinking. Both dielectric-confinement effect and network homogeneity were observed to be dependent on temperature and time of deswelling (Figure 11 and Figure S27). Water molecules associated with the

in  $\Delta\lambda$  from the beginning of deswelling (Figure 11) clearly suggests relatively fast volume phase transitions at elevated temperatures ( $60 > 45$  °C) by creating heterogeneous gel network in the early stage of deswelling. Similar observations in PL peak shift were made for NCH-2ME-0.5 (Figure S27). However, peak position of PL emission maxima for NCH-DDT-0.5 did not change noticeably with time at all temperatures (Figure S26), which could be attributed to the good compatibility between hydrophobic QDs and hydrophobic hydrogel networks formed above the VPT.

## CONCLUSIONS

RAFT polymerization of MEO<sub>2</sub>MA in the presence of DEGDMA as cross-linker and CDP as CTA was successfully conducted in DMF/toluene containing preformed CdS QDs to afford NCH. The enhancement in Mueller matrix-derived  $\delta$  and  $d$ -parameters for hpl-NCH (NCH-3MPA > NCH-2ME) with the doping concentration suggested improved structural/orientational order, and accordingly swelling ratios compared to OH of similar composition. This can be attributed to the H-bonding interactions between ethereal oxygen atoms of network pendant groups and QDs surface tethered  $-COOH/-OH$ , which was also in corroboration with high doping capacity and negligible QDs leakage. Opposite trends were observed for NCH-DDT and NCH-bulk because of relatively weak hydrophobic and lack of functional interactions between QDs and hydrogel matrix. The swelling induced  $\delta$ -parameter and quenching in PL intensity for swollen hydrogels in comparison with dry gels were proportional to the swelling ratios of NCH. The deswelling curves obtained by gravimetric analysis and fluorimetry were qualitatively similar and further corroborated with Mueller matrix-derived %  $\delta_R$  parameter. The combined result reveals overall deswelling process for all NCH and was slower at 45 and 60 °C, compared to 30 °C as a result of skin layer formation. The enhancement in skin layer formation and slow dehydration of collapsing network due to the rigid H-bonded network retarded deswelling for hpl-NCH (NCH-3MPA > NCH-2ME), with the doping concentration compared to OH. However, lower water retention values and %  $\delta_R$  ( $t = 120$  min) demonstrated the accelerated deswelling in case of NCH-DDT, ascribed to the formation of water leakage channels and DDT-mediated hydrophobic aggregation during network dehydration. Thus, the results presented above demonstrate that the hydrogel network structure, swelling ratio, PL properties, and deswelling process can be tuned by embedding different doping concentrations of either hydrophilically or hydrophobically modified QDs. Embedding CdS QDs in thermoresponsive PMEO<sub>2</sub>MA matrices endows luminescent properties to the resulting smart NCH, which could find plausible applications in thermo-optic imaging sensors and multifunctional drug delivery systems,<sup>63,64</sup> benefited from proposed tunable parameters.

## ASSOCIATED CONTENT

### Supporting Information

Detailed synthetic procedures of QDs, OH, and NCH, the optical properties of QDs in solution (Table S1), Mueller matrix-derived  $\delta$  and  $d$ -parameters for dry and swollen hydrogels (Figures S1–S10), cartoon representation of OH hydrogel structure in dry, swollen and deswollen state (Scheme S1), PL spectra of dry and swollen NCH (Figures S11–S12). Gravimetric deswelling plots for OH, NCH-2ME, and NCH-bulk (Figures S13–S14), Mueller matrix-derived  $\delta$ -parameter

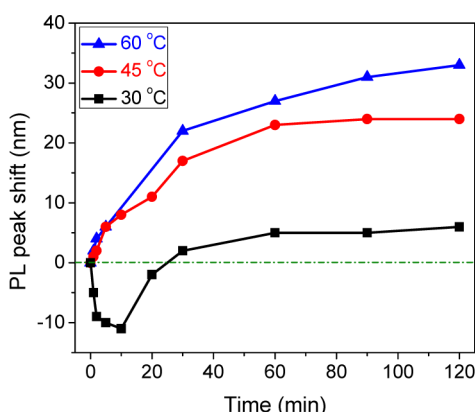


Figure 11. PL peak shift, upon deswelling for NCH-3MPA-0.5 at different temperatures.

hydrogel matrices diffuse out above VPT, thereby randomizing the hydrogel networks (low value of  $\delta$ -parameter at deswelling time  $t = 120$  min compared to  $t = 0$ , Table 1 and 2). Uniformly dispersed QDs in the homogeneous hydrogel network becomes close-packed due to shrinking (Scheme 1). Energy transfer (between different sized QDs) in close-packed crystals perhaps caused red-shift in PL peak position, which was also supported by narrowing of emission spectra with time upon deswelling. The initial decrease in PL peak shift ( $\Delta\lambda = \lambda_t - \lambda_0$ ) at 30 °C (Figure 11, deswelling time = 10 min) reveals further stabilization of the QDs by hydrophobic pockets created by collapsed hydrogel networks, and slow volume phase transitions through quasi-static equilibrium between water molecules and QDs mediated dehydration of networks.<sup>26</sup> Thereafter, close-packing of QDs in the heterogeneous network leads to the apparent red-shift in PL peak position. This phenomenon at 30 °C is further supported by a minimum PL shift (at deswelling time  $t = 120$  min) of 6 nm compared to 24 and 33 nm shifts at 45 and 60 °C, respectively (Figure 11). Interestingly, increase

for deswelling hydrogels (Figures S15–S19), gravimetric deswelling plots for NCH-2ME and NCH-bulk at 45 and 60 °C (Figures S20–S21), PL spectra of NCH-3MPA-0.5 during deswelling (Figure S22), fluorimetric deswelling plots for NCH-2ME-0.5 and NCH-bulk-0.5 (Figure S23), PL spectra of NCH-2ME-0.5, NCH-bulk-0.5 and NCH-DDT-0.5 during deswelling (Figures S24–S26), and the PL peak shift plot for NCH-2ME-0.5 upon deswelling (Figure S27). This material is available free of charge via the Internet at <http://pubs.acs.org>.

## ■ AUTHOR INFORMATION

### Corresponding Author

\*Telephone: +91 9674629345. E-mail: p\_de@iiserkol.ac.in (P.D.).

### Notes

The authors declare no competing financial interest.

## ■ ACKNOWLEDGMENTS

This work was supported by the Department of Science and Technology (DST), New Delhi, India [Project No.: SR/S1/OC-51/2010]. We also thank Jalpa Soni and Dr. Nirmalya Ghosh (Department of Physical Sciences, IISER, Kolkata) for helping us with the Mueller matrix polarimetry measurements.

## ■ REFERENCES

- (1) Vermonden, T.; Censi, R.; Hennink, W. E. Hydrogels for Protein Delivery. *Chem. Rev.* **2012**, *112*, 2853–2888.
- (2) Jonker, A. M.; Lowik, D. W. P. M.; van Hest, J. C. M. Peptide- and Protein-Based Hydrogels. *Chem. Mater.* **2012**, *24*, 759–773.
- (3) Wang, J. Z.; Loh, K. P.; Wang, Z.; Yan, Y. L.; Zhong, Y. L.; Xu, Q. H.; Ho, P. C. Fluorescent Nanogel of Arsenic Sulfide Nanoclusters. *Angew. Chem., Int. Ed.* **2009**, *48*, 6282–6285.
- (4) Taylor-Pashow, K. M. L.; Della Rocca, J.; Huxford, R. C.; Lin, W. Hybrid Nanomaterials for Biomedical Applications. *Chem. Commun.* **2010**, *46*, 5832–5849.
- (5) Weissman, J. M.; Sunkara, H. B.; Asher, S. A. Thermally Switchable Periodicities and Diffraction from Mesoscopically Ordered Materials. *Science* **1996**, *274*, 959–960.
- (6) Holtz, J. H.; Asher, S. A. Polymerized Colloidal Crystal Hydrogel Films as Intelligent Chemical Sensing Materials. *Nature* **1997**, *389*, 829–832.
- (7) Chen, C. W.; Akashi, M. Synthesis, Characterization, and Catalytic Properties of Colloidal Platinum Nanoparticles Protected by Poly(*N*-isopropylacrylamide). *Langmuir* **1997**, *13*, 6465–6472.
- (8) Sheeney-Haj-Ichia, L.; Sharabi, G.; Willner, I. Control of the Electronic Properties of Thermosensitive Poly(*N*-isopropylacrylamide) and Au-Nanoparticle/Poly(*N*-isopropylacrylamide) Composite Hydrogels upon Phase Transition. *Adv. Funct. Mater.* **2002**, *12*, 27–32.
- (9) Zrazhevskiy, P.; Sena, M.; Gao, X. H. Designing Multifunctional Quantum Dots for Bioimaging, Detection, and Drug Delivery. *Chem. Soc. Rev.* **2010**, *39*, 4326–4354.
- (10) Franceschi, S. D.; Kouwenhoven, L.; Schonenberger, C.; Wernsdorfer, W. Hybrid Superconductor–Quantum Dot Devices. *Nat. Nanotechnol.* **2010**, *5*, 703–711.
- (11) Kharlampieva, E.; Kozlovskaya, V.; Zavgorodnya, O.; Lilly, G. D.; Kotov, N. A.; Tsukruk, V. V. pH-responsive Photoluminescent LbL Hydrogels with Confined Quantum Dots. *Soft Matter* **2010**, *6*, 800–807.
- (12) Cheng, Z.; Liu, S.; Beines, P. W.; Ding, N.; Jakubowicz, P.; Knoll, W. Rapid and Highly Efficient Preparation of Water-Soluble Luminescent Quantum Dots via Encapsulation by Thermo- and Redox-Responsive Hydrogels. *Chem. Mater.* **2008**, *20*, 7215–7219.
- (13) Zhao, Y. J.; Zhao, X. W.; Tang, B. C.; Xu, W. Y.; Li, J.; Hu, L.; Gu, Z. Z. Quantum-Dot-Tagged Bioresponsive Hydrogel Suspension Array for Multiplex Label-Free DNA Detection. *Adv. Funct. Mater.* **2010**, *20*, 976–982.
- (14) Han, S.; Hagiwara, M.; Ishizone, T. Synthesis of Thermally Sensitive Water-Soluble Polymethacrylates by Living Anionic Polymerizations of Oligo(ethylene glycol) Methyl Ether Methacrylates. *Macromolecules* **2003**, *36*, 8312–8319.
- (15) Ali, M. M.; Stover, H. D. H. Well-Defined Amphiphilic Thermosensitive Copolymers Based on Poly(ethylene glycol monomethacrylate) and Methyl Methacrylate Prepared by Atom Transfer Radical Polymerization. *Macromolecules* **2004**, *37*, 5219–5227.
- (16) Sugihara, S.; Kanaoka, S.; Aoshima, S. Double Thermosensitive Diblock Copolymers of Vinyl Ethers with Pendant Oxyethylene Groups: Unique Physical Gelation. *Macromolecules* **2005**, *38*, 1919–1927.
- (17) Zhang, D.; Macias, C.; Ortiz, C. Synthesis and Solubility of (Mono-) End-Functionalized Poly(2-hydroxyethyl methacrylate-g-ethylene glycol) Graft Copolymers with Varying Macromolecular Architectures. *Macromolecules* **2005**, *38*, 2530–2534.
- (18) Lutz, J.-F.; Akdemir, O.; Hoth, A. Point by Point Comparison of Two Thermosensitive Polymers Exhibiting a Similar LCST: Is the Age of Poly(NIPAM) Over? *J. Am. Chem. Soc.* **2006**, *128*, 13046–13047.
- (19) Lutz, J.-F.; Hoth, A. Preparation of Ideal PEG Analogues with a Tunable Thermosensitivity by Controlled Radical Copolymerization of 2-(2-Methoxyethoxy)ethyl Methacrylate and Oligo(ethylene glycol) Methacrylate. *Macromolecules* **2006**, *39*, 893–896.
- (20) Skrabania, K.; Kristen, J.; Laschewsky, A.; Akdemir, O.; Hoth, A.; Lutz, J.-F. Design, Synthesis, and Aqueous Aggregation Behavior of Nonionic Single and Multiple Thermoresponsive Polymers. *Langmuir* **2007**, *23*, 84–93.
- (21) Lutz, J.-F. Polymerization of Oligo(ethylene glycol) (meth)-acrylates: Toward New Generations of Smart Biocompatible Materials. *J. Polym. Sci., Part A: Polym. Chem.* **2008**, *46*, 3459–3470.
- (22) Lutz, J.-F. Thermo-Switchable Materials Prepared Using the OEGMA-Platform. *Adv. Mater.* **2011**, *23*, 2237–2243.
- (23) Badi, N.; Lutz, J.-F. PEG-based Thermogels: Applicability in Physiological Media. *J. Controlled Release* **2009**, *140*, 224–229.
- (24) Fechler, N.; Badi, N.; Schade, K.; Pfeifer, S.; Lutz, J.-F. Thermogelation of PEG-Based Macromolecules of Controlled Architecture. *Macromolecules* **2009**, *42*, 33–36.
- (25) Lutz, J.-F.; Weichenhan, K.; Akdemir, O.; Hoth, A. About the Phase Transitions in Aqueous Solutions of Thermoresponsive Copolymers and Hydrogels Based on 2-(2-methoxyethoxy)ethyl Methacrylate and Oligo(ethylene glycol) Methacrylate. *Macromolecules* **2007**, *40*, 2503–2508.
- (26) Yoon, J. A.; Gayathri, C.; Gil, R. R.; Kowalewski, T.; Matyjaszewski, K. Comparison of the Thermoresponsive Deswelling Kinetics of Poly(2-(2-methoxyethoxy)ethyl methacrylate) Hydrogels Prepared by ATRP and FRP. *Macromolecules* **2010**, *43*, 4791–4797.
- (27) Yoon, J. A.; Kowalewski, T.; Matyjaszewski, K. Comparison of Thermoresponsive Deswelling Kinetics of Poly(oligo(ethylene oxide) methacrylate)-Based Thermoresponsive Hydrogels Prepared by “Graft-from” ATRP. *Macromolecules* **2011**, *44*, 2261–2268.
- (28) Patil, N.; Soni, J.; Ghosh, N.; De, P. Swelling-Induced Optical Anisotropy of Thermoresponsive Hydrogels Based on Poly(2-(2-methoxyethoxy)ethyl methacrylate): Deswelling Kinetics Probed by Quantitative Mueller Matrix Polarimetry. *J. Phys. Chem. B* **2012**, *116*, 13913–13921.
- (29) Yoshida, R.; Uchida, K.; Kaneko, Y.; Sakai, K.; Kikuchi, A.; Sakurai, Y.; Okano, T. Comb-Type Grafted Hydrogels with Rapid Deswelling Response to Temperature Changes. *Nature* **1995**, *374*, 240–242.
- (30) Chen, J.; Park, K. Synthesis and Characterization of Superporous Hydrogel Composites. *J. Controlled Release* **2000**, *65*, 73–82.
- (31) Serizawa, T.; Wakita, K.; Akashi, M. Rapid Deswelling of Porous Poly(*N*-isopropylacrylamide) Hydrogels Prepared by Incorporation of Silica Particles. *Macromolecules* **2002**, *35*, 10–12.
- (32) Zhang, J. T.; Huang, S. W.; Xue, Y. N.; Zhuo, R. X. Poly(*N*-isopropylacrylamide) Nanoparticle-Incorporated PNIPAAm Hydrogels with Fast Shrinking Kinetics. *Macromol. Rapid Commun.* **2005**, *26*, 1346–1350.

- (33) Kato, N.; Sakai, Y.; Shibata, S. Wide-Range Control of Deswelling Time for Thermosensitive Poly(N-isopropylacrylamide) Gel Treated by Freeze-Drying. *Macromolecules* **2003**, *36*, 961–963.
- (34) Haraguchi, K.; Takehisa, T. Nanocomposite Hydrogels: A Unique Organic–Inorganic Network Structure with Extraordinary Mechanical, Optical, and Swelling/De-swelling Properties. *Adv. Mater.* **2002**, *14*, 1120–1124.
- (35) Haraguchi, K.; Farnworth, R.; Ohbayashi, A.; Takehisa, T. Compositional Effects on Mechanical Properties of Nanocomposite Hydrogels Composed of Poly(*N,N*-dimethylacrylamide) and Clay. *Macromolecules* **2003**, *36*, 5732–5741.
- (36) Bekiari, V.; Pagonis, K.; Bokias, G.; Lianos, P. Study of Poly(*N,N*-dimethylacrylamide) /CdS Nanocomposite Organic/Inorganic Gels. *Langmuir* **2004**, *20*, 7972–7975.
- (37) Ghosh, N.; Wood, M.; Vitkin, I. A. Influence of the Order of the Constituent Basis Matrices on the Mueller Matrix Decomposition-Derived Polarization Parameters in Complex Turbid Media such as Biological Tissues. *Opt. Commun.* **2010**, *283*, 1200–1208.
- (38) Ghosh, N.; Vitkin, I. A. Tissue Polarimetry: Concepts, Challenges, Applications, and Outlook. *J. Biomed. Opt.* **2011**, *16*, 110801–110829.
- (39) Soni, J.; Purwar, H.; Ghosh, N. Quantitative Polarimetry of Plasmon Resonant Spheroidal Metal Nanoparticles: A Mueller Matrix Decomposition Study. *Opt. Commun.* **2011**, *285*, 1599–1607.
- (40) Hall, S. A.; Hoyle, M.-A.; Post, J. S.; Hore, D. K. Combined Stokes Vector and Mueller Matrix Polarimetry for Materials Characterization. *Anal. Chem.* **2013**, *85*, 7613–7619.
- (41) Chen, S.; Zhu, J.; Shen, Y.; Hu, C.; Chen, L. Synthesis of Nanocrystal–Polymer Transparent Hybrids via Polyurethane Matrix Grafted onto Functionalized CdS Nanocrystals. *Langmuir* **2007**, *23*, 850–854.
- (42) Khomane, R. B.; Manna, A.; Mandale, A. B.; Kulkarni, B. D. Synthesis and Characterization of Dodecanethiol-Capped Cadmium Sulfide Nanoparticles in a Winsor II Microemulsion of Diethyl Ether/AOT/Water. *Langmuir* **2002**, *18*, 8237–8240.
- (43) Pal, S. K.; Narayanan, S. S. Aggregated CdS Quantum Dots: Host of Biomolecular Ligands. *J. Phys. Chem. B* **2006**, *110*, 24403–24409.
- (44) Young, A. G.; Green, D. P.; McQuillan, A. J. Infrared Spectroscopic Studies of Monothiol Ligand Adsorption on CdS Nanocrystal Films in Aqueous Solutions. *Langmuir* **2006**, *22*, 11106–11112.
- (45) Adhikari, B.; Banerjee, A. Facile Synthesis of Water-Soluble Fluorescent Silver Nanoclusters and Hg<sup>II</sup> Sensing. *Chem. Mater.* **2010**, *22*, 4364–4371.
- (46) Rossetti, R.; Ellison, J. L.; Gibson, J. M.; Brus, L. E. Size Effects in the Excited Electronic States of Small Colloidal CdS Crystallites. *J. Chem. Phys.* **1984**, *80*, 4464–4469.
- (47) Moffitt, M.; Eisenberg, A. Size Control of Nanoparticles in Semiconductor-Polymer Composites. 1. Control via Multiplet Aggregation Numbers in Styrene-Based Random Ionomers. *Chem. Mater.* **1995**, *7*, 1178–1184.
- (48) He, R.; Qian, X.; Yin, J.; Xi, H.; Bian, L.; Zhu, Z. Formation of Monodispersed PVP-Capped ZnS and CdS Nanocrystals Under Microwave Irradiation. *Colloids Surf. A* **2003**, *220*, 151–157.
- (49) Bai, S.; Nguyen, T. -L.; Mulvaney, P.; Wang, D. Using Hydrogels to Accommodate Hydrophobic Nanoparticles in Aqueous Media via Solvent Exchange. *Adv. Mater.* **2010**, *22*, 3247–3250.
- (50) Noro, A.; Higuchi, K.; Sageshima, Y.; Matsushita, Y. Preparation and Morphology of Hybrids Composed of a Block Copolymer and Semiconductor Nanoparticles via Hydrogen Bonding. *Macromolecules* **2012**, *45*, 8013–8020.
- (51) Bai, S.; Wu, C.; Gawlitza, K.; Von Klitzing, R.; Ansorge-Schumacher, M.; Wang, D. Using Hydrogel Microparticles To Transfer Hydrophilic Nanoparticles and Enzymes to Organic Media via Stepwise Solvent Exchange. *Langmuir* **2010**, *26*, 12980–12987.
- (52) Millon, L. E.; Nieh, M. P.; Hutter, J. L.; Wan, W. SANS Characterization of an Anisotropic Poly(vinyl alcohol) Hydrogel with Vascular Applications. *Macromolecules* **2007**, *40*, 3655–3662.
- (53) Chen, S.; Hu, C.; Chen, L.; Xu, N. Facile Fabrication of Superhydrophobic Surface from Micro/Nanostructure Metal Alkane-thiolate Based Films. *Chem. Commun.* **2007**, *19*, 1919–1921.
- (54) Nieciecka, D.; Krysinski, P. Interactions of Doxorubicin with Self-Assembled Monolayer-Modified Electrodes: Electrochemical, Surface Plasmon Resonance (SPR), and Gravimetric Studies. *Langmuir* **2011**, *27*, 1100–1107.
- (55) Koole, R.; Liljeroth, P.; de Mello Donega, C.; Vanmaekelbergh, D.; Meijerink, A. Electronic Coupling and Exciton Energy Transfer in CdTe Quantum-Dot Molecules. *J. Am. Chem. Soc.* **2006**, *128*, 10436–10441.
- (56) Kokado, K.; Nagai, A.; Chujo, Y. Poly( $\gamma$ -glutamic acid) Hydrogels with Water-Sensitive Luminescence Derived from Aggregation-Induced Emission of *o*-Carborane. *Macromolecules* **2010**, *43*, 6463–6468.
- (57) Gou, M.; Jiang, M. Supramolecular Hydrogels with CdS Quantum Dots Incorporated by Host–Guest Interactions. *Macromol. Rapid Commun.* **2010**, *31*, 1736–1739.
- (58) Inomata, H.; Goto, S.; Saito, S. Phase Transition of N-Substituted Acrylamide Gels. *Macromolecules* **1990**, *23*, 4887–4888.
- (59) Okano, T.; Bae, Y. H.; Jacobs, H.; Kim, S. W. Thermally On-Off Switching Polymers for Drug Permeation and Release. *J. Controlled Release* **1990**, *11*, 255–262.
- (60) Kaneko, Y.; Nakamura, S.; Sakai, K.; Aoyagi, T.; Kikuchi, A.; Sakurai, Y.; Okano, T. Rapid Deswelling Response of Poly(*N*-isopropylacrylamide) Hydrogels by the Formation of Water Release Channels Using Poly(ethylene oxide) Graft Chains. *Macromolecules* **1998**, *31*, 6099–6105.
- (61) Peng, Z. A.; Peng, X. Mechanisms of the Shape Evolution of CdSe Nanocrystals. *J. Am. Chem. Soc.* **2001**, *123*, 1389–1395.
- (62) Li, J.; Hong, X.; Liu, Y.; Li, D.; Wang, Y. W.; Li, J. H.; Bai, Y. B.; Li, T. Highly Photoluminescent CdTe/Poly(*N*-isopropylacrylamide) Temperature-Sensitive Gels. *J. Adv. Mater.* **2005**, *17*, 163–166.
- (63) Li, X.; Li, H.; Liu, G.; Deng, Z.; Wu, S.; Li, P.; Xu, Z.; Xu, H.; Chu, P. K. Magnetic Loaded Fluorine-Containing Polymeric Micelles for Magnetic Resonance Imaging and Drug Delivery. *Biomaterials* **2012**, *33*, 3013–3024.
- (64) Shen, J.-M.; Tang, W.-J.; Zhang, X.-L.; Chen, T.; Zhang, H.-X. A Novel Carboxymethyl Chitosan-Based Folate/Fe<sub>3</sub>O<sub>4</sub>/CdTe Nanoparticle for Targeted Drug Delivery and Cell Imaging. *Carbohydr. Polym.* **2012**, *88*, 239–249.